Nano Lett., 2014, 14 (11), pp 6660–6665

High efficiency second harmonic generation from a single hybrid ZnO nanowire / Au plasmonic nano-oligomer

Gustavo Grinblat[1,2], Mohsen Rahmani[3], Emiliano Cortés[3], Martín Caldarola[1], David Comedi[2], Stefan A. Maier[3] and Andrea V. Bragas[1*]*

[1] Laboratorio de Electrónica Cuántica, Dep. de Física, FCEN, Universidad de Buenos Aires, Intendente Güiraldes 2160, C1428EGA Buenos Aires, Argentina – IFIBA CONICET, Argentina

[2] Laboratorio de Física del Sólido, Dep. de Física, FACET, Universidad Nacional de Tucumán, Av. Independencia 1800, 4000 Tucumán, Argentina – CONICET, Argentina

[3] The Blackett Laboratory, Department of Physics, Imperial College London, London SW7 2AZ, United Kingdom

* Corresponding Authors: s.maier@imperial.ac.uk; bragas@df.uba.ar

ABSTRACT. We introduce a plasmonic-semiconductor hybrid nanosystem, consisting of a ZnO nanowire coupled to a gold pentamer oligomer by crossing the hot-spot. It is demonstrated that the hybrid system exhibits a second harmonic (SH) conversion efficiency of ~3x10^{-5}%, which is among the highest values for a nanoscale object at optical frequencies reported so far. The SH intensity was found to be ~1700 times larger than that from the same nanowire excited outside the hot-spot. Placing high nonlinear susceptibility materials precisely in plasmonic confined-field regions to enhance SH generation, opens new perspectives for highly efficient light frequency up-conversion on the nanoscale.

KEYWORDS. Plasmonic nano-oligomer, ZnO nanowire, field enhancement, photonic-plasmonic coupling, second harmonic generation (SHG).

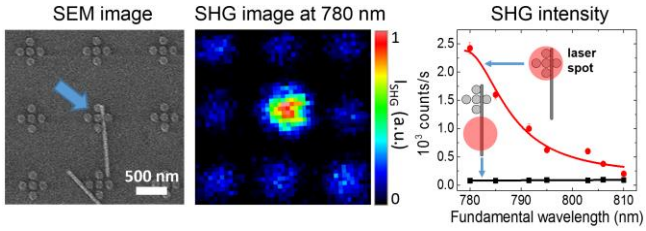

The fabrication of devices having high optical frequency up-conversion efficiencies in nanoscale volumes is very desirable for a large number of applications, ranging from the development of optoelectronic hybrid systems [1], to (bio)imaging [2, 3] and sensing [4, 5], amongst others. Since nonlinear processes based on photon–photon interactions are essentially weak and, in addition to that, phase matching is not possible at subwavelength scales, many strategies have been tested in order to enhance the generation of harmonics [6, 7]. Ideally, any approach adopted to address this problem should consider the choice of materials with large nonlinear susceptibilities as well as producing high and confined incident fields. In this context, metallic plasmonic nanostructures are key elements for focusing free-space light into nanometer-scale

volumes [8, 9]. However, the coupling of efficient materials for second harmonic generation (SHG) with high-field regions generated by plasmonic nanoantennas, still remains challenging.

In the dipolar approximation, SHG coming from the bulk is forbidden in centrosymmetric materials; therefore SHG is dominated by quadrupolar bulk terms and surface contributions (which vanish for spherical shape [10]). However, the presence of inhomogeneities in the fields and/or in the materials at the nanoscale may induce a high second order nonlinear response, even in the case of centrosymmetric structures and spherical shapes [10-12]. A system consisting of nanostructured metals excited at the plasmon resonances is a highly inhomogeneous one with enhanced fields concentrated in very small volumes. For these reasons, these kinds of plasmonic nanoantennas have been used themselves as harmonic generators with significant efficiencies [6, 7, 13-19]. Different designs have produced SH conversion efficiencies as high as 10^{-7}-10^{-6} % [13-15]. Interesting reported alternatives consist in combining nonlinear thin films with arrays of plasmonic nanostructures [20-22] or covering a nonlinear nanomaterial with a plasmonic shell [23]. With these approaches, SHG intensity enhancements of up to 1600 times [21] were achieved with respect to the bare nonlinear material. Regarding the SH conversion efficiency, similar values to those for bare metallic nanoantennas (without intrinsic nonlinear surrounding) have been found [20], but for lower excitation power.

In a more complex approach, SH could be generated by placing a suitable nonlinear nanomaterial precisely where the field is enhanced (i.e. in the gaps of a metallic nanoantenna), which is much more challenging technologically [24]. Strategies like this have been used to enhance the photoluminescence (PL) from a quantum dot [25], accelerate the emission from a dye molecule [26], control the resonance wavelength of a nanoantenna [27], subwavelength plasmonic mapping [28, 29], and produce enhanced third harmonic emission from an ITO

nanoparticle coupled to a nanoantenna [30, 31]. However, so far, this approach has not yet been applied to efficiently generate SH light.

In this Letter, we introduce a new hybrid system consisting of a single ZnO nanowire (NW), which is a non-centrosymmetric material with high nonlinear susceptibility, coupled to a plasmonic Au pentamer acting as the nanoantenna. We demonstrate that a NW conveniently located at the plasmonic hot-spot allows obtaining a SH conversion efficiency of ~$3x10^{-5}$%. The SH enhancement factor reaches values of up to 1700 and varies with the wavelength of the fundamental beam so as to follow the spectral profile of the SH generated by the pure nanoantenna.

For the development of hybrid nanostructures, we first fabricated arrays of Au pentamers by electron beam lithography on a fused silica substrate, as shown in the scanning electron microscope (SEM) image of Figure 1(a) (see SI section 1 for fabrication details). Dimensions and gap size of Au pentamers were designed to achieve a plasmonic resonance at ~780 nm, as shown (red dashed curve) in Figure 1(b). Simulations were obtained by a three-dimensional finite-difference time domain technique (FDTD) using the commercial software FDTD Solution v8.6 (Lumerical). As it can be seen, the experimental extinction spectrum for the pentamer array (black solid line in Figure 1(b)) is in good agreement with theory (see SI section 4 for more information about optical measurements). The capability of these plasmonic oligomers to generate hot-spots by focusing light into nanoscale gaps [32-34] is shown in Figure 1(c). This image exhibits the simulated near-field intensity ($|E(x,y)^2|/|E_0^2|$) distribution for circularly polarized incident light at resonance (λ = 780 nm) showing four regions with very high power density. The horizontal component of the excitation field is responsible for the lateral bright spots (left and right), while the pentamer interaction with the vertical component produces the

other two (top and bottom) [35]. Enhancement factors of the field intensity of up to ~100 are calculated inside the 20 nm size gap regions between Au disks. Therefore, the use of circularly polarized incident light to resonantly excite a pentamer, leads to four suitable locations where ZnO NWs can be placed.

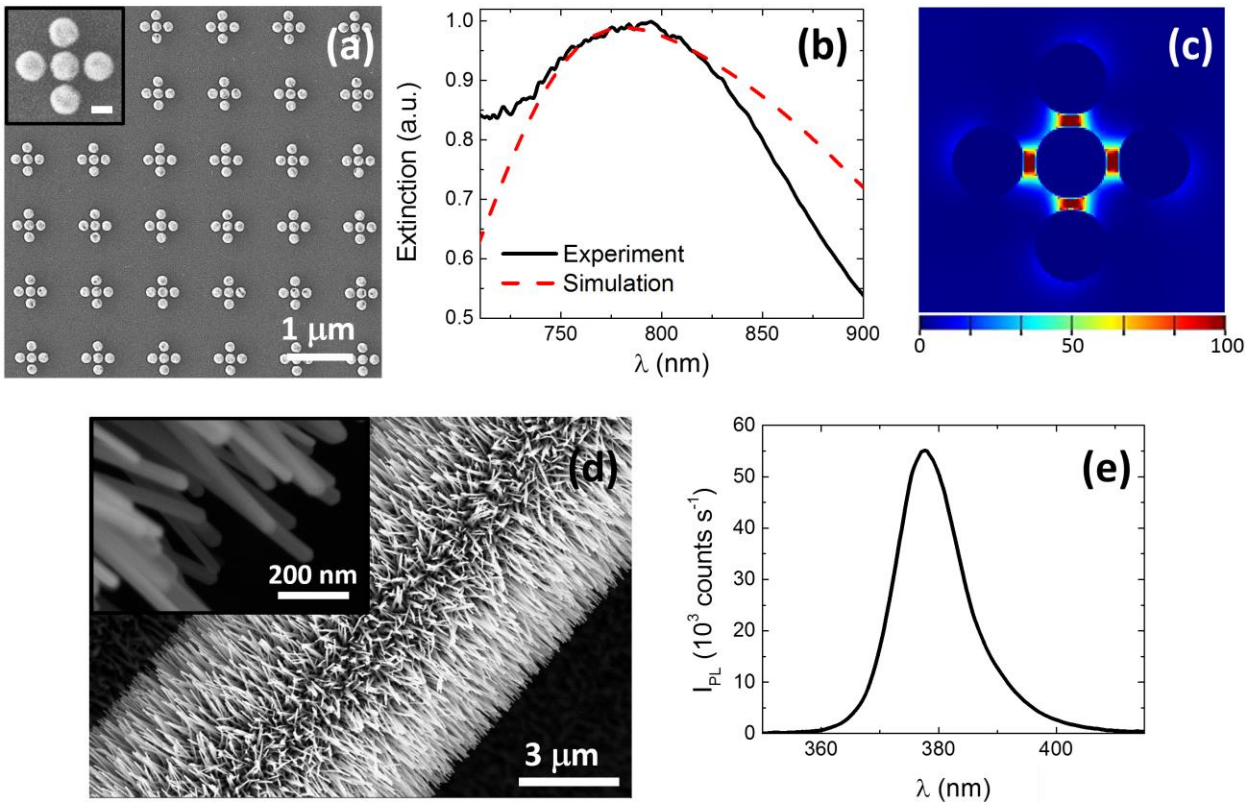

Figure 1. (a) SEM image of the pentamer array. Inset shows a magnified view of a single pentamer. Scale bar, 100 nm. **(b)** Experimental and simulated extinction spectrum of the pentamers in the near-infrared region. **(c)** Calculated near-field intensity distribution in the pentamer at λ = 780 nm for circularly polarized incident light. **(d)** SEM image of the as-grown ZnO NWs. The inset shows a magnified view of the main Figure. **(e)** PL spectrum from the NWs. The peak at 378 nm corresponds to ZnO excitonic emission.

Fabrication of ZnO NWs was performed via vapor transport and deposition (VTD) [36] over commercial carbon fiber fabric (see SI section 2 for details). Figure 1(d) shows a SEM image of a portion of carbon fiber fully covered with ZnO NWs. Dimensions of the obtained NWs are 1-2 μm length with a ~30 nm diameter. The PL spectrum from the sample is shown at Figure 1(e).

Typical ZnO excitonic band-gap emission centered at 378 nm is observed. We aim to combine these ZnO nanostructures with the nanoantennas at the individual level. Since NWs are micrometric in length, this would allow optical characterization of the NW in and outside hot-spot regions. The NW lengths serve as a probe for evaluating the field intensity enhancement.

In order to obtain physical insight into SHG from the hybrid system, it is complementary to gain understating about SH emission of the distinct components, which will serve as a reference characterization. SH measurements were performed in a home-made confocal microscope, which is schematized in Figure 2(a), fed with a Ti:Sapphire (Ti:Sa) pulsed laser of 50 fs pulse width and 90 MHz repetition rate. The Ti:Sa laser wavelength ($\lambda_{exc.}$) was tuned from 780 nm to 810 nm, so that twice the energy of the pumping photon (390 nm to 405 nm) is always below the ZnO band-gap (see Figure 1(e)), where the SHG is the main light emission process against the two photon photoluminescence (TPPL) [36-38]. Note that the mentioned $\lambda_{exc.}$ range includes the plasmonic resonance wavelength of the pentamers (780 nm). To study ZnO NWs individually, they were transferred from the carbon fibers to a clean substrate by a dry printing process, which consisted of gently pressing the samples against each other. The receiving substrate results covered with NWs that lie parallel to the substrate surface plane but randomly oriented within that plane. As ZnO is a birefringent material, the intensity of the generated SH for a NW will depend on the input polarization. In the case of linearly *s* or *p* polarized light, their corresponding SH relative intensities will be determined by the adequate relation between *d333* and *d311* elements of the second-order nonlinear optical tensor of ZnO, where the index *3* labels the c-axis, which is in the direction of the NW main axis [39]. In order to avoid differences in the SH emission intensities due to polarization effects, the laser polarization was set to be circular.

Hence, any detected variations in SH intensity emission between different isolated ZnO NWs should be associated with differences between NW volumes.

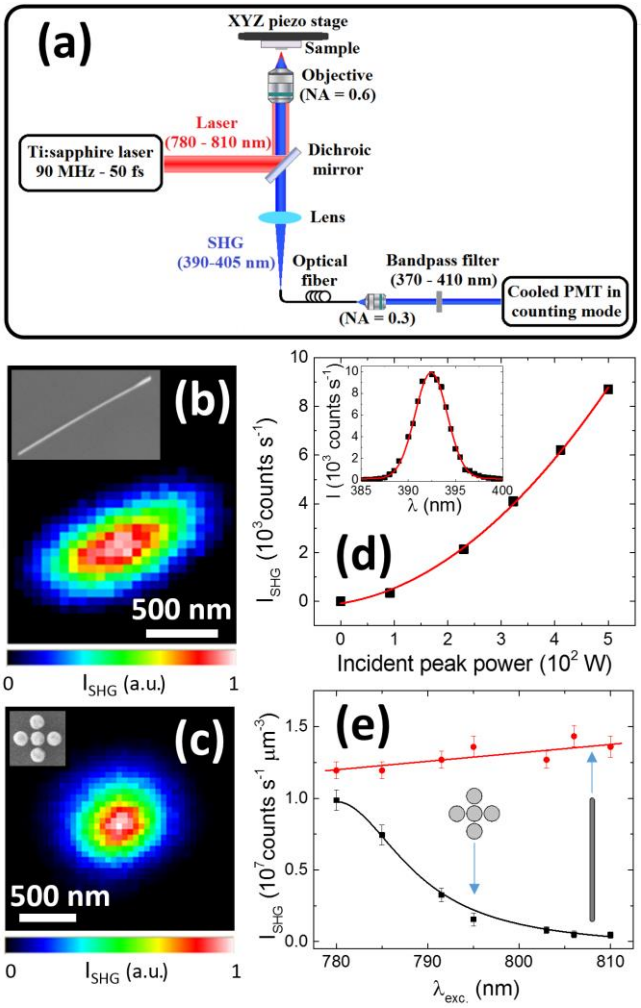

Figure 2. (a) Simplified schematic of the home-made confocal microscope employed for the SHG intensity measurements. SHG and SEM (inset) images of a single ZnO NW **(b)** and pentamer **(c)**. $\lambda_{exc.}$ = 785 nm. **(d)** SHG intensity as a function of the incident peak power for a ZnO NW. Red line is a fit with a second-order power function. The inset shows the SHG spectrum of a single NW at $\lambda_{exc.}$ = 785 nm. **(e)** SHG intensity of non-interacting pentamer and NW for different excitation wavelengths. The data are normalized by the volume of the nanostructures.

SH images of the nanostructures were produced using an integration time per scanning pixel of 1-10 ms, while for measurements at fixed positions it was increased up to 500 ms. Figures 2 (b) and (c) show SH images for $\lambda_{exc.}$ = 785 nm of a single ZnO NW and Au pentamer, respectively

(corresponding SEM images in insets). The excitation spot was about 700 nm diameter over the sample (full width at half maximum), while the lateral resolution achieved at the SH wavelength was around 450 nm. Figure 2(d) shows the dependence of the SHG intensity on the incident peak power, which is found to be quadratic as shown by the fit. The inset in that figure exhibits the SHG spectrum from a single NW, showing a Gaussian peak centered at $\lambda_{exc.}/2$ with ~2 nm half width at half maximum. The dependence of the SHG intensity (I_{SHG}) on the excitation wavelength for both nanostructures can be appreciated in Figure 2(e). These results are averages from several individual measurements on similar nanostructures. To enable comparison between the two, the I_{SHG} data in Figure 2(e) were normalized by the corresponding excited volume (which is about 7 times larger for the nanoantenna than for the NW). The excitation average power density was set to $2x10^5$ W/cm^2 with a corresponding peak intensity of $6x10^{10}$ W/cm^2. While for the NW I_{SHG} varies no more than a 20% within the studied wavelength range, for the pentamer it decreases monotonically from 780 nm to 810 nm, as it is detuned from the plasmonic resonance. A Lorentzian function centered at 780 nm was used to fit the data from the nanoantenna. A similar resonant-like behavior has been recently described for third harmonic generation in Au nanoparticles dimmers [31].

After characterizing the SHG from isolated NW and pentamers, we now turn our attention to the hybrid system. Sample preparation involved transferring ZnO NWs to the nanoantenna substrate, and NWs crossing plasmonic gap regions were studied. We note that the pentamer structure chosen quadruples the number of hot-spots with respect to typical dimer-like configuration, substantially increasing the probability of turning bare nanoantennas into coupled nanosystems after the NWs transfer process (see SI section 3 for more discussion and details). Figure 3(a) shows a SEM image of a 3x3 pentamer array with ZnO NWs. The 9 pentamers will be called as

their corresponding (i,j) coordinates in the array, with i,j =1, 2, 3 running from left to right and from bottom to top, respectively. As it can be seen from the image, for the (2,2) nanoantenna positioned in the middle, a ZnO NW lies across its gap on the right side. Since the diameter of this NW is 35 nm (which is larger than the 20 nm gap size), it is expected to be on top of the pentamer. When the Ti:Sa laser is tuned to the plasmonic resonance (780 nm), the SH emission coming from the NW at the gap region is found to be significantly larger than that from the NW outside the gap. This can be appreciated in the SH image in Figure 3(b), recorded at the same zone as in Figure 3(a). The SHG intensity from the middle region of the NW is negligible compared to that from its top part. Additionally, emission coming from the bare nanoantennas is about one order of magnitude lower than that from the hybrid nanostructure (see SI section 5 for the data). It is worth mentioning that the bottom part of the NW is very close to the (2,1) pentamer. The same occurs for the other NW located at the bottom in Figure 3(a). However, since none of these NWs are exactly in gap regions of the (2,1) nanoantenna, no enhancement effect is noticed. When the excitation is detuned from the resonance to 805 nm (Figure 3(c)), SH emission from the hybrid nanostructure lowers about a factor of 5, while the middle part of the main NW as well as the NW at the bottom appear faintly in the image. In order to further demonstrate the role of the hot-spot in the enhancement of the SHG for our hybrid system, we present some off-resonance measurements in the SI (section 6) showing weak emission.

Figure 3(d) shows the SHG intensity from the main NW measured at the (2,2) nanoantenna region and over the NW middle part as a function of $\lambda_{exc.}$. I_{SHG} differs by a factor of up to ~40 between both curves. However, this factor should be corrected by the area of the NW that is excited in each case, which is very different. The excited area of the NW when the laser is focused onto the nanoantenna is much smaller than when the excitation is performed over the

bare NW, since for the first case the light is confined at the gap zone. The enhancement factor of the SHG intensity for the ZnO NW ($f_{SHG\text{-}NW}$) is defined as the ratio between the upper and lower curves from Figure 3(d) (subtracting first the small contribution of the bare nanoantenna from the upper curve), after normalizing each data set by the corresponding excitation surface area. Figure 3(e) shows the dependence of $f_{SHG\text{-}NW}$ on λ_{exc} (black squares), which reaches a value of ~1700 for 780 nm. The red triangles in Figure 3(e) are the data corresponding to the pentamer alone in Figure 2(f) multiplied by a constant. Very good agreement between both curves is obtained. This can be interpreted as that the SH emission from the bare nanoantenna measures the profile of the square of the intensity enhancement at the gap regions. Thus the NW serves as an efficient probe of the hot-spot intensity enhancement. Moreover, it has been reported that the extinction spectrum of a nanoantenna changes when other material is approached, and as a consequence a wavelength shift in the resonance can be found [27, 30, 31]. However, for a ZnO NW placed on top of the pentamer, no significant shift is expected for the Au oligomer plasmonic resonance (see inset of Figure 3(e)).

We have performed numerical simulations to study the field enhancement probed by the NW at the nanoantenna when it is excited at resonance. For this analysis, a hexagonal transverse section was assumed for the NW [36, 37]. Different orientations of the hexagonal face over the pentamer gap as well as different shapes (i.e. cylindrical) for the NW produced similar results. Regarding the SH generated by the NW at the gap, we note that the nanoantenna should not affect significantly the angular distribution of the emission, since near ~400 nm, though it exhibits some absorption, the extinction cross section of the pentamer is minimum.

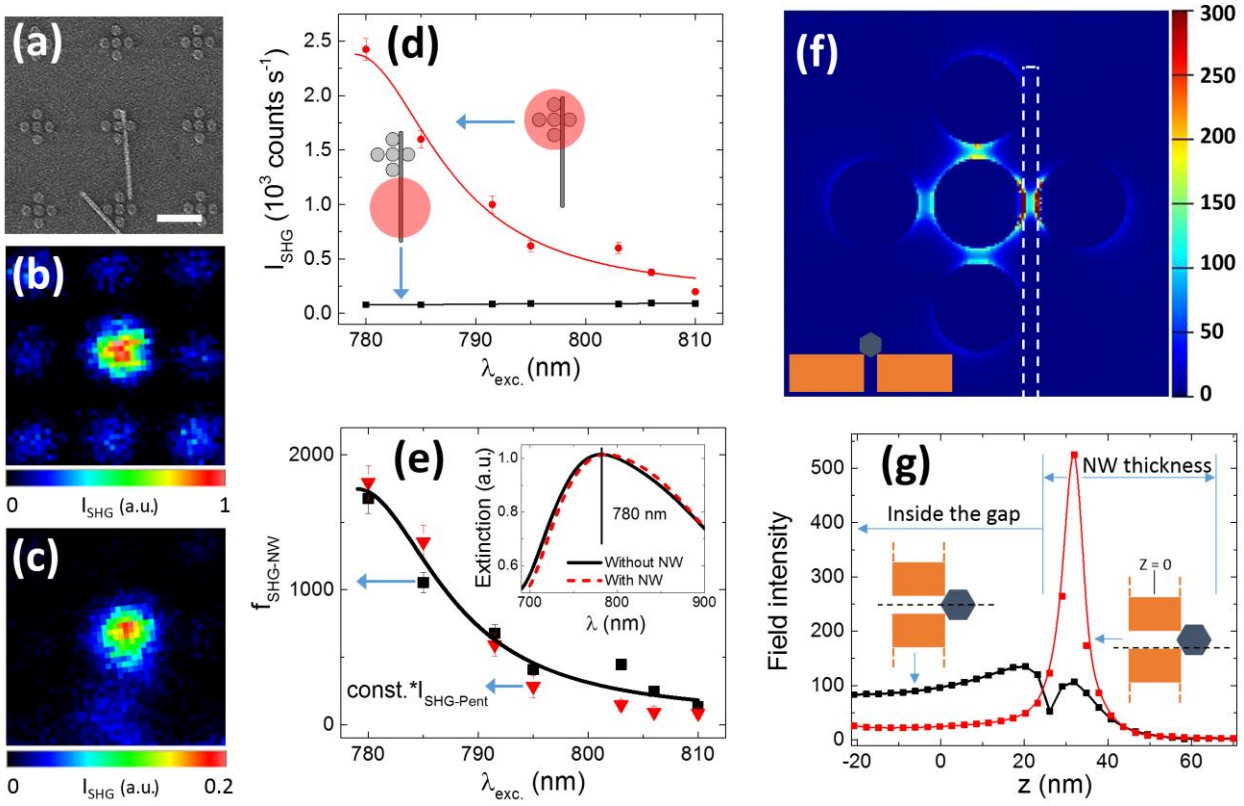

Figure 3. (a) SEM image of a 3x3 array of nanoantennas with ZnO NWs. The pentamer in the middle of the picture is traversed by a NW at its gap on the right. Scale bar, 500 nm. **(b)** and **(c)** are SHG images of the region shown in (a) excited at $\lambda_{exc.}$ = 780 nm and $\lambda_{exc.}$ = 805 nm respectively. **(d)** SHG intensity of the hybrid nanostructure excited at the nanoantenna and below it over the NW. **(e)** Black squares: enhancement factor of the SHG intensity for the ZnO NW (f_{SHG-NW}) for different excitation wavelengths. The profile of f_{SHG-NW} is comparable to that of the SHG intensity of an individual pentamer ($I_{SHG-Pent}$). The inset shows the simulated extinction spectra of the pentamer with and without the NW. **(f)** Calculated near-field intensity distribution in the hybrid nanostructure at the nanoantenna top for circularly polarized incident light at resonance. The sketch at the bottom left is a schematic cross section view of the NW at the gap zone. **(g)** Field intensity along the z axis for the gap on the right in (f) for the gap center and the gap's right edge. z = 0 corresponds to the half-height of the pentamer.

Figure 3(f) shows the simulated near-field intensity distribution for the hybrid system at the top of the nanoantenna. Significant intensity enhancement of ~100 (~500) is found at the center (lateral edges) of the gap region crossed by the NW. These values would signify a SH increase on the order of 10^4-10^5. However, not all the NW in depth is excited at such high intensities in that zone. Figure 3(g) exhibits the field intensity along the z axis (perpendicular to the sample surface) at the center of the gap and also at one of its lateral edges. It is observed that only a

minor amount of the NW senses an enhanced electric field at the gap region. This reduces the mentioned factor for the SH emission intensification to ~10^3-10^4, which is comparable to the experimental effective value of SHG enhancement found at the plasmonic resonance ($f_{SHG\text{-}NW}$ ~1700). We note, that if we had made the gap wider so the NW could fit within (in width and height), the volume of excited material would have been maximum, but the excitation field enhancement would have been much lower. Our calculations predict that $(|E(x,y)^2|/|E_0^2|)^2$ at the hot-spot would drop by a factor of ~10 for a 40 nm gap, resulting in a similar SH enhancement with respect to the bare NW. On the other hand, if we consider a NW narrow enough to fit within the 20 nm gap (as a 15 nm diameter NW), simulations of the field distribution give similar enhancement values as those in figure 3(f), but show no increase in the amount of excited semiconductor material. Therefore, this would not improve the SHG efficiency.

It must be mentioned, that since *d311* is reported to be a few times smaller than *d333* for ZnO nanostructures [40, 41], the measured value of $f_{SHG\text{-}NW}(\lambda_{exc.})$ constitutes a lower bound. The component of the excitation field that is focused onto the NW at the pentamer gap is the horizontal one. On the other hand, the main contribution to the SH emission from the middle part of the NW is produced by the vertical component of the excitation field, since the c-axis of the ZnO NW is almost parallel to this direction. In view of this, we should consider whether a NW crossing the same gap but oriented perpendicularly, would lead to the highest SH emission. However, the comparison is not trivial, since for the last case no portion of the NW would penetrate the gap (independently of the NW diameter), so the volume of excited material would become reduced. In addition, the larger area of contact between Au and ZnO that would arise, could increase optical damping (caused by absorption of the nanoantenna at the SH wavelength)

and raise the temperature of the semiconductor (due to ohmic losses in the metal), deteriorating the performance of the plasmonic-photonic nanosystem.

Finally, we measured the SHG efficiency of the hybrid nanostructure, obtaining a very high value of ~$3x10^{-5}$%, calculated normalizing the emission by the geometric cross section of the nanoantenna. We note that, potentially, with the four gaps of a pentamer crossed by NWs, this efficiency value could be increased to ~$1x10^{-4}$%.

In summary, we have introduced a new route to generate efficiently second harmonic light at the nanoscale, by placing a ZnO NW in the hot spot of a plasmonic oligomer. Direct observation of the SH light coming out of such a hybrid sample using a confocal microscope, allowed us to carefully quantify the SH efficiency and field enhancement. To the best of our knowledge, the ~$3x10^{-5}$% of SHG efficiency is among the highest values reported so far at the nanoscale for optical frequencies.

ASSOCIATED CONTENT

Supporting information (SI) is accessible in the online version. This material is available free of charge via the Internet at http://pubs.acs.org.

AUTHOR INFORMATION

Corresponding Authors

bragas@df.uba.ar and s.maier@imperial.ac.uk

Notes

The authors declare no competing financial interest.

ACKNOWLEDGMENT

We thank Dr. R. Oulton for fruitful discussions. The authors acknowledge funding provided by grants from Universidad de Buenos Aires (20020100100719), ANPCyT (Préstamo BID PICT Nº 2010-00825), the Leverhulme Trust and the UK Engineering and Physical Sciences Research Council (EPSRC).

REFERENCES

(1) Van Sark, W. GJHM; de Wild, J.; Rath, J. K.; Meijerink, A.; Schropp, R. E. I. *Nanoscale Res. Lett.* **2013**, *8*, 81.
(2) Ang, L. Y.; Lim, M. E.; Ong, L. C.; Zhang, Y. *Nanomedicine* **2011**, *6*, 1273-1288.
(3) Bautista, G.; Huttunen, M. J.; Mäkitalo, J.; Kontio, J. M.; Simonen, J.; Kauranen, M. *Nano Lett.* **2012**, *12*, 3207-3212.
(4) Chen, J.; Zao, J. X. *Sensors* **2012**, *12*, 2414-2435.
(5) Butet, J.; Martin, O. J. F. *ACS Nano* **2014**, *8*, 4931-4939.
(6) Kauranen, M.; Zayats, A. V.; *Nat. Photonics* **2012**, *6*, 737-748.
(7) Hasan, S. B.; Lederer, F.; Rockstuhl, C. *Mater. Today* **2014**, http://dx.doi.org/10.1016/j.mattod.2014.05.009.
(8) Halas, N. J.; Lal, S.; Chang, W.-S.; Link, S.; Nordlander, P. *Chem. Rev.* **2011**, *111*, 3913-3961.
(9) Giannini, V.; Fernández-Domínguez, A. I.; Heck, S. C.; Maier, S. A. *Chem. Rev.* **2011**, *111*, 3888-3912.
(10) Brudny, V. L.; Mendoza, B. S.; Mochán, W. L.; *Phys. Rev. B* **2000**, *62*, 11152-11162.
(11) Berthelot, J.; Bachelier, G.; Song, M.; Rai, P.; des Francs, G. C.; Dereux, A.; Bouhelier, A. *Opt. Exp.* **2012**, *20*, 10498-10508.
(12) Canfield, B. K.; Kujala, S.; Jefimovs, K.; Turunen, J.; Kauranen, M. *Opt. Exp.* **2004**, *12*, 5418-5423.
(13) Zhang, Y.; Grady, K. G.; Ayala-Orozco, C.; Halas, N. J. *Nano Lett.* **2011**, *11*, 5519-5523.
(14) Aouani, H.; Navarro-Cia, M.; Rahmani, M.; Sidiropoulos, T. P. H.; Hong, M.; Oulton R. F.; Maier S. A. *Nano Lett.* **2012**, *12*, 4997-5002.
(15) Park, S.; Hahn, J. W.; Lee, J. Y. *Opt. Exp.* **2012**, *20*, 4856-4870.
(16) Klein, M. W.; Enkrich, C.; Wegener, M.; Linden, S. *Science* **2006**, *313*, 502-504.
(17) Metzger, B.; Schumacher, T.; Hentschel, M.; Lippitz, M.; Giessen, H. *ACS Photonics* **2014**, *1*, 471-476.
(18) Thyagarajan, K.; Rivier, S.; Lovera, A.; Martin, O. J. F. *Opt. Exp.* **2012**, *20*, 12860-12865.
(19) Thyagarajan, K.; Butet, J.; Martin, O. J. F. *Nano Lett.* **2013**, *13*, 1847-1851.
(20) Ding, Wei; Zhou, L.; Chou, S. Y. *Nano Lett.* **2014**, *14*, 2822-2830.
(21) Chen, K.; Durak, C.; Heflin, J. R., Robinson, H. D. *Nano Lett.* **2007**, *7*, 254-258.
(22) Harutyunyan, H.; Volpe, G.; Quidant, R.; Novotny, L. *PRL* **2012**, *108*, 217403.
(23) Richter, J.; Steinbrück, A.; Zilk, M.; Sergeyev, A.; Pertsch, T.; Tünnermann, A.; Grange, A. *Nanoscale* **2014**, *6*, 5200-5207.
(24) Casadei, A.; Pecora, E.F.; Trevino, J.; Forestiere, C.; Rüffer, D.; Russo-Averchi, E.; Matteini, F.; Tutuncuoglu, G.; Heiss, M.; i Morral, A. F.; Dal Negro, L. *Nano Lett.* **2014**, *14*, 2271-2278.

(25) Bermúdez Ureña, E.; Kreuzer, M. P.; Itzhakov, S.; Rigneault, H.; Quidant, R.; Oron, D.; Wenger, *J. Adv. Mater.* **2012**, *24*, OP314-OP320.
(26) Busson, M. P.; Rolly, B.; Stout, B.; Bonod, N.; Bidault, S. *Nat. Commun.* **2012**, *3*, 962.
(27) Liu, N.; Wen, F.; Zhao, Y.; Wang, Y.; Nordlander, P.; Halas, N. J.; Alú, A. *Nano Lett.* **2013**, *13,* 142-147.
(28) Koller, D. M.; Hohenester, U.; Hohenau, A.; Ditlbacher, H.; Reil, F.; Galler, N.; Aussenegg, F. R.; Leitner, A.; Trügler, A.; Krenn, J. R. *PRL* **2010**, *104*, 143901.
(29) Dregely, D.; Neubrech, F.; Duan, H.; Vogelgesang, R.; Giessen, H. *Nat. Commun.* **2013**, *4*, 2237.
(30) Aouani, H.; Rahmani, M.; Navarro-Cía, M.; Maier, S. A. *Nature Nanotech.* **2014**, *9*, 290-294.
(31) Metzger, B.; Hentschel, M.; Schumacher, T.; Lippitz, M.; Ye, X.; Murray, C. B.; Knabe, B.; Buse, K.; Giessen, H. *Nano Lett.* **2014**, *14*, 2867-2872.
(32) Rahmani, M.; Yoxall, E.; Hopkins, B.; Sonnefraud, Y.; Kivshar, Y.; Hong, M.; Philips, C.; Maier, S. A.; Miroshnichenko, A. E. *ACS Nano* **2013**, *7*, 11138-11146.
(33) Rahmani, M.; Lukiyanchuk, B.; Tahmasebi, T.; Lin, Y..; Liew, T. Y. F.; Hong, M. H. *Appl. Phys. A* **2011**, *107*, 23-30.
(34) Ye, J.; Wen, F.; Sobhani, H.; Lassiter, J. B.; Van Dorpe, P.; Nordlander, P.; Halas, N. J. *Nano Lett.* **2012**, *12*, 1660-1667.
(35) Rahmani, M.; Lukiyanchuk, B.; Ng, B.; Tavakkoli, K. G., A.; Liew, Y. F.; Hong, M. H. *Opt. Exp.* **2011**, *19*, 4949-4956.
(36) Grinblat, G.; Capeluto, M. G.; Tirado, M.; Bragas, A. V.; Comedi, D. *Appl. Phys. Lett.* **2012**, *100*, 233116.
(37) Capeluto, M. G.; Grinblat, G.; Tirado, M.; Comedi, D.; Bragas, A. V. *Opt. Exp.* **2014**, *22*, 5341-5349.
(38) Pedersen, K.; Fisker, C.; Pedersen, T. G. *Phys. Stat. Sol.* **2008**, *5*, 2671-2674.
(39) Vega, N. C.; Wallar, R.; Caram, J.; Grinblat, G.; Tirado, M.; LaPierre, R. R.; Comedi, D. *Nanotechnology* **2012**, *23*, 275602.
(40) Geren, K.; Liu, S. W.; Zhou, H. J.; Zhang, Y.; Tian, R.; Xiao, M. *Jour. of Appl. Phys.* **2009**, *105*, 063531.
(41) Johnson, J. C.; Yan, H.; Schaller, R. D.; Petersen, P. B.; Yang, P.; Saykally, R. J. *Nano Lett.* **2002**, *2*, 279-283.